Morphogen and community effects determine cell fates in response to BMP4 signaling in human embryonic stem cells

Anastasiia Nemashkalo[1], Albert Ruzo[2], Idse Heemskerk[1], and Aryeh Warmflash[1,3,*]

Affiliations:

[1]Department of Biosciences and [3]Department of Bioengineering, Rice University, Houston, TX 77005.

[2]Laboratory of Stem Cell Biology and Molecular Embryology, The Rockefeller University, New York, New York 10065

* Correspondence to AW: aryeh.warmflash@rice.edu.

Abstract:

Paracrine signals maintain developmental states and create cell-fate patterns in vivo, and influence differentiation outcomes in human embryonic stem cells (hESCs) in vitro. Systematic investigation of morphogen signaling is hampered by the difficulty of disentangling endogenous signaling from experimentally applied ligands. Here, we grow hESCs in micropatterned colonies of 1-8 cells ("μColonies") to quantitatively investigate paracrine signaling and the response to external stimuli. We examine BMP4-mediated differentiation in μColonies and standard culture conditions and find that in μColonies, above a threshold concentration, BMP4 gives rise to only a single cell fate, contrary to its role as a morphogen in other developmental systems. Under standard culture conditions, BMP4 acts as morphogen, but this effect requires secondary signals and particular cell densities. We further find that a "community effect" enforces a common fate within μColonies both in the state of pluripotency and when cells are differentiated, and that this effect allows more precise response to external signals. Using live cell imaging to correlate signaling histories with cell fates, we demonstrate that interactions between neighbors result in sustained, homogenous signaling necessary for differentiation.

Keywords: human embryonic stem cells, micropatterning, BMP4 pathway, differentiation mechanisms

Summary Statement (15-30 words): We quantitatively examined signaling and differentiation in hESC colonies of varying size treated with BMP4. We show that secondary signals result in morphogen and community effects that determine cell fates.

Introduction

Morphogen signaling pathways control cell fate during embryonic development, and can be manipulated to produce particular fate outcomes in human embryonic stem cells (hESCs). During development, all signals both originate from, and are received by, the cells of the embryo, however, cultured cells combine extrinsic influences from the culture medium with endogenous signals passed between cells. In hESCs, secondary signals often perturb the outcome of directed differentiation (Kurek et al., 2015; Warmflash et al., 2014; Yu et al., 2011). Whether endogenous signals are required to maintain particular states, such as the pluripotent state, or to ensure the robustness of differentiation into coherent territories has not been investigated in hESCs. Dissecting the effects of paracrine signals from responses to external stimuli would enable researchers to harness endogenous signals to achieve particular aims, and aid in dissecting the role of these signals in the developing embryo.

The BMP pathway is a conserved morphogen signaling pathway that regulates dorsal-ventral patterning in species from flies to mammals (Bier and De Robertis, 2015) and has also been shown to be essential for mammalian gastrulation (Arnold and Robertson, 2009; Winnier et al., 1995). However, the difficulty in obtaining quantitative data has prevented determining whether BMP functions as a morphogen during mammalian gastrulation. Interestingly, in hESCs, there is increasing evidence that treatment with BMP4 leads to trophectodermal (Horii et al., 2016; Li et al., 2013; Xu et al., 2002) and mesodermal fates (Kurek et al., 2015; Warmflash et al., 2014; Yu et al., 2011), and that the mesodermal fates may be lost when Wnt, Nodal, or FGF signaling is inhibited. Although there is abundant molecular data supporting the identity of these hESC-derived trophoectodermal cells, it has remained controversial (reviewed in (Li and Parast, 2014)) as the correlates of hESCs, the cells of the epiblast, do not give rise to trophoectodermal lineages, and data showing that hESC derived trophoblast cells can function in vivo are also lacking.

When colony geometries are controlled, BMP4 can trigger formation of patterns containing trophectoderm and all three embryonic germ layers (Etoc et al., 2016; Warmflash et al., 2014). These patterns arise in response to homogeneous treatment with BMP4 because of secondary paracrine signals that are required for producing and positioning the mesendodermal

30   territories (Warmflash et al., 2014). Under these culture conditions in which cells are housed

31   within large colonies, it is difficult to disentangle the direct response to the BMP signal from the

32   effects of interactions between the cells (Bernardo et al., 2011). It is therefore unclear whether

33   the different fates induced by BMP4 treatment depend on the dose of BMP4 and, if so, if cells

34   directly read the BMP4 concentration. Quantitative dissection of the cellular response to supplied

35   BMP4 as well as any paracrine interactions that function in the state of pluripotency or during

36   BMP4-mediated differentiation could resolve these important issues.

37   Here we use a micropatterning approach to isolate the effects of BMP treatment from the

38   secondary endogenous signals that are active both in the state of pluripotency and during BMP-

39   mediated differentiation. To do so, we confined cells to very small colonies ranging from one to

40   eight cells (from here on referred to as µColonies), allowing us to compare isolated cells, which

41   respond only to the exogenous signaling, with cells housed within increasing large colonies

42   where the contribution of paracrine signaling increases. Our results show that, in this context,

43   BMP4 does not act as morphogen but instead functions as a switch and, above a threshold,

44   induces only the trophectodermal fate. In contrast, in standard culture conditions in which

45   colonies may consist of hundreds or thousands of cells, BMP4 elicits both mesodermal and

46   trophectodermal fates in a dose-dependent manner that also requires Nodal signaling and

47   particular cell densities. Further, we find the main effect of secondary signals on the short length

48   scales in µColonies is to enforce a common fate within the colony. This enforcement allows cells

49   to more faithfully remain pluripotent in conditions supporting this state and to differentiate

50   sensitively and homogenously in response to external stimuli. We show that this enforcement is

51   the result of more sustained BMP signaling in larger colonies sizes, and that in standard culture

52   conditions, the outcome of BMP mediated differentiation correlates with the duration of the

53   BMP signal rather than the initial response.

54   **Results**

55   **BMP4 produces nearly pure populations of trophectodermal cells in µColonies.** We first

56   optimized cell seeding such that nearly all µColonies contain between 1 and 8 cells (Fig. 1A,B).

57   Cells in µColonies grown for 42 hours in the pluripotency supporting media MEF-CM expressed

58   the pluripotency markers SOX2, OCT4, and NANOG (Fig. S1 A-C). In the experiments below,

59   we used SOX2 protein expression levels as a marker for hESC pluripotency but show that Nanog

60   obeys similar trends (see Fig. S2). We next assayed the response of µColonies to a range of

61   BMP4 concentrations (0.1-30 ng/ml for 42 hours).

62   In response to increasing BMP4 levels, cells within µColonies transitioned from pluripotent

63   (SOX2+) to a differentiated fate expressing CDX2 and GATA3 and lacking expression of

64   BRACHYURY, SOX17, EOMES, NANOG and SOX2 (Fig. S1D-E and Fig. 1C). Consistent

65   with a growing body of literature on BMP4-mediated differentiation (Horii et al., 2016; Li and

66   Parast, 2014; Xu et al., 2002), we identify these cells as trophectoderm, and below we use CDX2

67   as a marker for this fate. Besides CDX2 and GATA3, all other differentiation markers were

68   detected in less than 2% of cells in the population, and in all conditions, nearly the entire

69   population of cells expressed either the SOX2 marker of pluripotency or the CDX2

70   differentiation marker. We detected almost no BRA+ cells at any dose (Fig. 1C). BMP4 doses of

71   0.1 - 0.3 ng/ml produced mixtures of SOX2+ and CDX2+ cells while those at 1 ng/ml or higher

72   yielded nearly pure populations of CDX2+ with complete downregulation of SOX2 expression

73   (Fig. 1D). In contrast, previous literature has shown that larger colonies differentiate to a

74   heterogeneous mixture of fates even in response to much higher doses of BMP4 (Tang et al.,

75   2012; Warmflash et al., 2014). These results establish that cells in µColonies differentiate more

76   sensitively and homogenously than cells in standard-sized colonies in response to BMP4 ligand,

77   and suggest that arrays of small colonies like the ones we employ here may have utility in

78   directed differentiation schemes.

79   **In standard culture, BMP elicits a morphogen effect that depends on Nodal signaling and**

80   **cell density.** To better understand the lack of mesodermal differentiation in µColonies, we

81   compared the differentiation outcomes in response to a similar range of BMP4 doses for cells

82   grown without confinement to small colonies. We used the pan-mesodermal and primitive-streak

83   marker BRA to determine the extent of mesodermal differentiation. We seeded cells such that

84   the density was homogenous throughout the culture dish and varied this density (see below). We

85   observed a morphogen effect in that the cell fate depended on the concentration of BMP4. Below

86   2 ng/ml BMP4, cells remained in the SOX2+ pluripotent state, at 2-4 ng/ml cells differentiated to

87   BRA+ mesodermal cells reaching a maximum of approximately 30% BRA positive cells with

88   the remainder CDX2 positive, while at higher doses cells primarily adopted a CDX2+BRA-

89   trophoectodermal fate (Fig. 2A top row, Fig. 2B and Fig. S3A-C).

90   If cells directly read the BMP4 concentration, inhibitors of other signaling pathways

91   should not perturb the morphogen effect. We found that treatment with the Activin/Nodal

92   signaling inhibitor SB431542 abolished mesoderm differentiation at all doses so that cells

93   switched between only the SOX2+ and CDX2+ fates as in µColonies (Fig. 2A bottom row, Fig.

94   2C, Fig. S3D). This supports the idea that the morphogen effect in response to BMP4 requires

95   secondary signals. We next reasoned that the response to secondary signals should be density

96   dependent, and examined the role of cell density in differentiation outcomes. Indeed at the dose

97   of peak BRA induction (2 ng/ml), we only observed BRA-expression at 30 and 60 x 10^3

98   cells/cm^2 but not at lower or higher densities (Fig. 2D, Fig. S3E). At higher BMP4 doses, cells

99   did not express BRA at any cell density but primarily expressed CDX2 at low densities and

100   SOX2 at high densities (Fig. 2E, Fig. S3F). Note that at both 2 and 10 ng/ml BMP4 at high

101   densities, cells failed to differentiate and remained SOX2+, consistent with other reports that

102   BMP signaling and differentiation are inhibited at high cell densities (Etoc et al., 2016). Finally,

103   to explicitly confirm that activating the Activin/Nodal pathway together with BMP stimulation

104   would be sufficient to give rise to mesodermal differentiation, we compared µColonies treated

105   with BMP4 and Activin to those treated with BMP4 alone. Consistent with the above results, we

106   observed substantial mesodermal differentiation in colonies treated with BMP4 and Activin but

107   not in those treated with BMP4 alone (Figure S4). Thus, taken together, our results support a

108   model where only the CDX2 fate is a direct consequence of BMP4 signaling. Mesodermal

109   differentiation can also result at particular doses, but it requires secondary signaling through the

110   Activin/Nodal pathway, and is only induced at particular cell densities. In µColonies treated with

111   BMP-4 alone, cell numbers are likely too low to produce sufficient secondary Nodal signals to

112   induce mesodermal fates, but these can be induced by adding Activin to the media.

113   **A community effect enforces a common fate within µColonies in both pluripotent and**

114   **differentiation states.** We noted that in the µColony experiments above, even at BMP4

115   concentrations that produced mixtures of different fates (CDX2+ or SOX2+), the fates of cells

116   within an individual colony were highly correlated, while neighboring colonies often differed in

117   fate, suggesting reinforcement of a common fate within the µColony (Fig. 1D), a phemonenon

118   referred to as the community effect (Bolouri and Davidson, 2010; Gurdon, 1988). To investigate

119   whether a community effect is operating within µColonies, we examined the expression of the

120   SOX2 and CDX2 markers as a function of number of cells in the colony at varying BMP4 doses.

121   Interestingly, under pluripotency supporting conditions, expression of the pluripotency marker

122   SOX2 increased with colony size, while under differentiation conditions, expression of SOX2

123   decreased with colony size. The differentiation marker CDX2 showed opposite trends: a minor

124   population of spontaneously differentiated CDX2+ cells was observed in 1-cell colonies in

125   pluripotent conditions, and the fraction of CDX2+ cells decreased with colony size. In contrast,

126   the size of the CDX2+ population increased with colony size when differentiated with BMP4

127   (Fig. 1E-H and Fig. 3A-C). Comparing histograms of expression levels for all cells in the

128   experiment grown in colonies of a particular size under pluripotency conditions, we found a

129   population of cells in 1-cell colonies with reduced SOX2 and enhanced CDX2, and this

130   population was absent in larger colonies (Fig. 3B). This suggests that a fraction of cells

131   spontaneously differentiate to a distinct state and that this differentiation only occurs in colonies

132   with small numbers of cells. We also found similar distributions revealing distinct

133   subpopulations of differentiated and undifferentiated one-cell colonies in differentiation

134   conditions but with the opposite trend: pluripotent cells only persisted in colonies with smaller

135   numbers of cells (Fig. S5A-B). This second population of cells becomes increasingly rare as the

136   colony size increases (Fig. 3C, experimental data). We also confirmed this community effect in

137   a second hESC line (Fig. S5C,D) and that it does not depend on the presence of ROCK-inhibitor

138   in the culture media (Fig. S5E,F).

139   **A simple statistical-mechanical model quantitatively accounts for the community effect.**

140   The experiments above show that in the μColony system cells can be in one of two states –

141   pluripotent (SOX2+) or trophectodermal (CDX2+). Interactions between cells enforce a common

142   fate inside the colony, while externally supplied BMP4 can bias that common fate towards the

143   CDX2+ state. To explore whether these simple features are sufficient to explain the system's

144   behavior quantitatively, we exploited an analogy with the Ising model used in statistical physics

145   to describe a two-state system of atomic spins that are coupled to their neighbors and respond to

146   an external field. We made the simplifying assumption that every cell is coupled to every other

147   within a μColony, which is justified by the small colony sizes, and the extensive cell movements

148   we observe in the timelapse experiments below. Within this model, we explored the effects of

149   changing these parameters, and found that increasing either J or the number of cells in the colony

150   will increase the likelihood that all cells in the colony adopt the same fate. As expected,

151   increasing B lead to a general increase in the fraction of CDX2+ cells, with the transition being

152   gradual at low values of J and sharper at high values (Figure S6A-C).

153   To directly compare the model to data, we performed quantitative fitting of the fraction

154   of CDX2+ and SOX2+ cells as a function of colony size using a separate parameter for the value

155   of B and J at each concentration (see methods and Figure S6). The data for the fraction of cells in

156   each subpopulation as a function of colony size at different BMP4 concentrations was well fit

157   with this simple model (Fig. 3C, black curves). Further, other data not used in fitting the model,

158   such as the distribution of fates within μColonies of a particular size were predicted by the model

159   without further adjustment to the parameters (Fig. S6D). We also examined the fit values of the

160   parameters B and J as a function of the BMP4 concentration (Figure S6E). As expected, the

161   value of B increased with the BMP4 concentration reflecting the increased bias towards CDX2+

162   fates. Interestingly the value of J was nearly constant reflecting a similar tendency for cells to

163   adopt the same fate within a colony at all BMP4 concentrations. In fact, the data was fit equally

164   well with a model in which the value of J was assumed to be the same for all BMP4

165   concentrations (Figure S6E). Taken together, these results suggest that within μColonies BMP4

166   mediated differentiation can be quantitatively explained by only two features – the bias of

167   differentiation towards the trophectodermal fate that increases with BMP4 and the constant

168   coupling between neighboring cells that causes them to adopt the same fate.

169   **Proliferation rates and clonal composition do not explain the community effect.** A simple

170   hypothesis that would partially explain the observed community effect is that some cells are

171   already differentiated upon seeding. If these cells proliferate more slowly, then we would expect

172   colonies that began with differentiated cells would be on average smaller than those containing

173   pluripotent cells. This hypothesis would predict differences in cell cycle as a function of colony

174   size. That is, cells in smaller colonies would be more likely to be arrested in the G1 phase of the

175   cell cycle. To test this hypothesis, we first analyzed the integrated DAPI intensity as a proxy for

176   the total DNA content of the cells, and found that it did not vary with colony size in either

177   pluripotent or differentiation conditions (Fig. 4A). We next created hESCs expressing RFP-

178   Cdt1, a component of the FUCCI system that is expressed only in the G1 phase (Sakaue-Sawano

179   et al., 2008). No differences in the fraction of cells in G1 phase were observed between colonies

180   of different sizes in either pluripotent or differentiation conditions (Fig. 4B), We note that the

181 hypothesis that cell cycle differences underlie the community effect also could not explain our

182 results in the differentiated state where cells expressing pluripotency markers only persist in

183 small colonies.

184   To unambiguously establish whether cells within a colony may be more alike because

185 they are clonal derived, we performed an experiment in which we mixed 5% CFP-labeled and

186 95% unlabeled cells and evaluated their expression of SOX2 in pluripotent conditions or CDX2

187 in differentiation conditions. If our results can be explained by the clonal composition of

188 colonies, we would expect that most colonies in our experiments are clonally derived, and that in

189 colonies of mixed clones, there are larger differences in expression of markers such as SOX2 or

190 CDX2 between clones than within the cells of the same clone.   In larger colonies of 4-8 cells,

191 colonies with CFP-positive cells nearly always had CFP-negative cells as well indicating that

192 multiple clones are typically present despite the uniformity in CDX2 or SOX2 expression

193 (Figure 4C). Moreover, quantitatively, within colonies of mixed CFP positive and negative cells,

194 the mean expression of the CFP positive and negative clones were as correlated as groups of

195 equal numbers of cells in which the cells were chosen randomly without regard to clonal origin

196 (Figure 4D). Thus, these experiments conclusively exclude clonal expansion as an explanation

197 for the uniformity within a colony in either pluripotency or differentiation. Instead, we favor the

198 interpretation that single cells less robustly interpret the supplied signals than small colonies do

199 (see below), and that signaling enforces uniform differentiation within the colony. We also

200 investigated whether the community effect could be affected by modulating the pluripotency-

201 maintaining Activin/Nodal and FGF pathways (Fig. S7A-B) or inhibiting the differentiation-

202 promoting Wnt and BMP pathways (Fig. S7A-B), but we did not observe significant differences

203 in the community effect in any of these cases.

204 **During differentiation in μColonies, enforcement of sustained signaling underlies the**

205 **community effect.** We next turned to understanding the community effect observed during

206 BMP-mediated differentiation using a reporter cell line for the BMP signaling pathway. We used

207 CRISPR/Cas9 genome engineering to insert GFP at the endogenous locus to form an N-terminal

208 fusion with SMAD4, and isolated a clonal line with a heterozygous insertion of GFP (Fig. S9A-

209 C). Similar fusions have been shown to be faithful reporters of SMAD signaling in the past

210 (Schmierer and Hill, 2005; Sorre et al., 2014; Warmflash et al., 2012). We compared assaying

211   pathway activity with the GFP-SMAD4 reporter and with antibody staining for C-terminally

212   phosphorylated SMAD1/5/8 and found that they give similar dynamics at 1 and 10 ng/ml (Figure

213   S9D-E).

214   In undifferentiated cells, GFP-SMAD4 localizes to the cytoplasm and translocates to the

215   cell nucleus upon stimulation with BMP4 (Fig. 5A). We performed live confocal imaging

216   beginning approximately four hours before stimulation and quantified the BMP signaling

217   response by measuring the nuclear to cytoplasmic ratio of GFP-SMAD4 during differentiation

218   induced by 10 ng/ml BMP4 (Fig. 5A,B and Movie S1). To increase statistical power, we seeded

219   reduced numbers of cells in µColonies and focused only on the difference between 1 and 2 cell

220   colonies. We note that the designation of number of cells in the colony refers to the number of

221   cells at the time of stimulation. We observe both cell division and cell death in colonies of all

222   sizes, and the final number and the number at the time of stimulation will often differ.

223   The reporter revealed similar signaling intensities in 1 and 2 cell colonies before BMP4

224   stimulation and in the early response to the ligand up to 10 hours after stimulation. Thereafter,

225   the mean trajectories began to diverge with the two-cell colonies showing higher signaling (Fig.

226   5C). Examining the distribution of signals in individual cells, we found that this divergence in

227   the mean is mostly due to the presence of one cell colonies that revert to near baseline levels of

228   signaling, while this does not occur in two-cell colonies (Fig. 5D-F). Thus, we hypothesized that

229   cells without sustained signaling will fail to differentiate to CDX2+ cells while the high

230   signaling cells will differentiate.

231   To test this hypothesis directly, we performed live-cell imaging of one-cell colonies and

232   then fixed these colonies and analyzed their levels of CDX2. We defined cells as low or high

233   signaling depending on whether their temporal average overlapped with the distribution of

234   signaling before stimulation. We found that 75% of high signaling cells but only 31% of low

235   signaling cells differentiated to a CDX2+ cell fate (Fig. 5G). Differences in the mean signaling

236   intensities between CDX2 positive and negative cells became evident after the early phase of

237   response, similar to the differences between one and two cell colonies (Fig. 5H). To see whether

238   the cell cycle might play a role in these results, we also examined whether there were differences

239   in cell division depending on whether cells differentiated to a CDX2+ fate. Dividing and non-

240   dividing cells gave rise to CDX2+ cells in approximately equal proportions (Figure 5I). These

241 data are consistent with a mechanism by which cell-cell interactions serve to maintain the BMP

242 signaling response, perhaps by directly activating the BMP4 gene (Karaulanov et al., 2004;

243 Schuler-Metz et al., 2000), and thereby enforce differentiation to trophectodermal fates. One-cell

244 colonies that lack this reinforcement both signal and differentiate more heterogeneously.

245 **During differentiation in standard culture conditions, sustained signaling is required for**

246 **differentiation into CDX2 fate.** To investigate the relationship between BMP signaling

247 dynamics and differentiation more generally, we performed dose response experiments under

248 standard culture conditions using the same GFP-SMAD4 cell line. At each dose, we measured

249 the BMP signaling dynamics and then fixed the same cells and analyzed their differentiation to

250 CDX2+ trophectoderm. To avoid the complications of cells adopting multiple fates, we cultured

251 the cells with SB431542 in order to prevent mesodermal differentiation. Interestingly, in the

252 range of 1-10 ng/ml BMP4, the initial response to ligand stimulation was identical and the

253 trajectories only diverged at later time points with 1 ng/ml showing significant decay of the

254 signal and 3 ng/ml showing a small decay as compared to the cells at 10 ng/ml (Fig. 6A,B top

255 panel). These trends were mirrored in the differentiation data, cells at 1 ng/ml largely failed to

256 express CDX2 while those at 3 ng/ml expressed it almost as highly as those at 10 ng/ml (Fig. 6B,

257 bottom panel). Since the initial signaling response was the same in all cases, these data

258 demonstrate that the maintenance of signaling, rather than the magnitude of the initial response,

259 is the determining factor for whether cells will differentiate in response to BMP4.

260 To directly determine whether the initial response or prolonged signaling is responsible

261 for differentiation, we performed experiments in which we treated one group of cells with a high

262 concentration of BMP4 (10 ng/ml) that gave rise to differentiation and another group with a

263 lower one (1 ng/ml) that did not. After 3 hours, we switched the media between these two

264 groups, so that one group was switched from 1 to 10 ng/ml BMP4 while the other was switched

265 from 10 to 1 ng/ml. (Figure 6C). Consistent with a sustained response being required for

266 differentiation, cells initially stimulated with 10 ng/ml and then switched to 1 ng/ml had a

267 decline in signaling and did not differentiate to CDX2+ fates, while those switched from 1 ng/ml

268 to 10 ng/ml had sustained signaling and differentiated. Finally, to directly measure the effect of

269 signal duration on differentiation, we stimulated cells with a high dose of 10 ng/ml BMP4 and

270 then switched to media containing the BMP inhibitor Noggin (250 ng/ml) at variable times after

271 the initial stimulation. As measured by the GFP-SMAD4 reporter, switching from BMP4

272   containing media to Noggin containing media led to a rapid shutdown of signaling. Importantly,

273   only cells remaining in BMP4 for 42 hours differentiated to CDX2+ fates while those switched

274   to Noggin containing media at 3, 18, or 28 hours failed to differentiate (Figure 6D).

275   **Discussion**

276   Here we introduce a μColony system that allowed us to separately study exogenous and

277   paracrine signaling in hESCs quantitatively and with cellular resolution. We show that

278   endogenous signals enforce a common fate within the colony both in pluripotent conditions and

279   when differentiated with BMP4. This enforcement of a common fate allows larger μColonies to

280   respond more robustly to signals supplied in the growth media: sustaining pluripotency in

281   pluripotency supporting media and differentiating sensitively and homogenously in response to

282   the extrinsic differentiation signal. We show that under standard culture conditions, BMP4 acts

283   as a morphogen, inducing different fates in a concentration dependent-manner, while in

284   μColonies it switches cells from pluripotent to a single fate, trophectoderm, when supplied above

285   a threshold. This apparent discrepancy is due to the need for secondary signals to produce the

286   morphogen effect in standard culture conditions, and μColonies do not reach sufficient densities

287   to produce these secondary signals. We developed a mathematical model which shows that the

288   detailed statistics regarding the number of cells in the pluripotent or trophectodermal fate as a

289   function of colony size can be predicted from only two parameters: the strength of the bias

290   towards the trophectodermal fates by BMP4 and the strength the interactions between cells that

291   enforce a common fate.

292   The enforcement of a common fate and greater sensitivity to external signals was

293   observed in the induction of Xenopus animal cap cells to muscle fates by vegetal cells by Gurdon

294   who termed this phenomenon the "community effect" (Gurdon, 1988). This work showed that

295   individual animal cap cells inserted between two pieces of vegetal tissue failed to differentiate, in

296   contrast to larger aggregates that were induced to muscle fates. This suggested that interactions

297   between the animal cap cells are required to robustly interpret the mesoderm differentiation

298   signals emanating from the vegetal cells. In hESCs, cells at higher density have been shown to

299   better maintain pluripotency upon the withdrawal of pluripotency-maintaining cytokines, also

300   supporting the existence of a community effect promoting this state (Peerani et al., 2007). A

301   related observation has been made regarding the levels of Oct4 and Nanog in colonies of mESCs

302   grown in "ground state" conditions (Muñoz-Descalzo et al., 2012): the levels differ between

303   colonies but are highly similar between cells in the same colony suggesting reinforcement of

304   common levels through cellular communication. In theoretical work, Bolouri and Davidson

305   proposed that positive feedback of a signal upon its own transcription could underlie the

306   community effect and applied this idea to the maintenance of the oral ectoderm of the sea urchin

307   embryo through induction of *nodal* gene expression by Nodal signaling (Bolouri and Davidson,

308   2010). Another theoretical study also found that positive feedback on the signal was sufficient to

309   explain the community effect, and suggested that additional negative feedbacks must operate to

310   prevent the entire tissue from converting to a single fate (Saka et al., 2011). Similarly, in this

311   study, we find that the enforcement of sustained BMP signaling by interactions between the cells

312   is necessary for ensuring that all cells within the colony adopt the same trophectodermal fate.

313   During development, the community effect serves to ensure a common fate over

314   relatively short length scales, and thereby creates coherent territories of a single cell type.

315   Previous work in hESCs has shown that as colony size is increased, cell-fate patterns emerge

316   (Etoc et al., 2016; van den Brink et al., 2014; Warmflash et al., 2014). It is likely that the

317   community effect plays a role in ensuring the coherence of local territories, but other phenomena

318   must emerge on longer length scales to create these patterns. Future work on embryonic

319   patterning with stem cells can probe this transition to understand the emergence of self-organized

320   patterns.

321   Cells in μColonies of sufficient size differentiate homogenously in response to very low

322   concentrations of ligand. Here, concentrations of 1 ng/ml induced nearly pure populations of

323   CDX2+GATA3+ trophectoderm, whereas in larger colonies, nearly 100 fold greater

324   concentrations induce a mixture of different fates (Tang et al., 2012; Warmflash et al., 2014).

325   Thus, μColonies seeded at appropriate densities may represent a platform for sensitive and

326   robust directed differentiation.

327   Our results here suggest that only trophectodermal fates are directly induced from

328   epiblast cells by BMP4, and that it does not directly induce multiple fates in a dose-dependent

329   manner. Experiments with inhibiting secondary signals, modulating cell density, and comparing

330   μColonies to standard culture, establish that there is an apparent morphogen effect in treating

331   hESCs with BMP4, but that this is indirect, relying on secondary signals and only operating at

332   particular cell densities. The role of BMP4 in initiating gastrulation and mesendoderm

333   differentiation both in vivo (Winnier et al., 1995) and in vitro (Bernardo et al., 2011; Kurek et

334   al., 2015; Warmflash et al., 2014; Yu et al., 2011) requires other signals and was not seen in our

335   experiments at any BMP4 dose in μColonies. Our data suggest that that μColonies do not contain

336   sufficient cell numbers to initiate the secondary signals such as Nodal and Wnt that operate

337   during gastrulation in the mammalian embryo (Arnold and Robertson, 2009), and are important

338   for patterning pluripotent cells in vitro (Berge et al., 2008; Warmflash et al., 2014).

339   It will be interesting to use the methods established here to examine whether these other

340   developmental signaling pathways function directly as morphogens. In vivo evidence from

341   genetic perturbations suggests that Nodal signaling induces multiple different fates in a dose-

342   dependent manner during gastrulation (Dunn et al., 2004; Robertson, 2014), and the μColony

343   system could determine whether this is a direct result of cells reading out the Nodal signal or

344   whether other interactions are required. Similarly, as BMP4 has a documented role as a

345   morphogen in dorsal ventral patterning (Ferguson and Anderson, 1992; Tucker et al., 2008;

346   Wilson et al., 1997), it would be interesting to subject these systems to a similar analysis to

347   determine if cells are directly reading the BMP4 concentration in these cases.

348   **Author Contributions**

349   A.N., I.H., and A.W. designed experiments. A.N. performed experiments. A.N., I.H., and A.W.

350   performed analysis. A.W. supervised research. A. R. created the GFP-SMAD4 cell line. A.N and

351   A.W. wrote the paper.

352   **Materials and Methods**

353   **Cell Culture.** *Routine Culture.* For regular maintenance, hESCs were grown in mTeSR1 in

354   tissue culture dishes coated with Matrigel overnight at 4°C (dilution 1:200 in DMEMF12). Cells

355   were passaged using dispase every 3 days. Cells were routinely tested for mycoplasma

356   contamination. For imaging experiments under standard culture conditions, cells were seeded

357   onto 8- or 4-well imaging slides (ibidi) at densities of ~63 x10^3 cells per cm^2. For density

358   dependent experiments, the densities were varied as indicated.

359   *Micropatterned experiments.* We used the micropatterning protocol described in detail in

360   (Deglincerti et al., 2016) with adjusted cell numbers. Briefly, micropatterning experiments were

361   performed using HUESM conditioned by mouse embryonic fibroblasts and supplemented with

362 20ng/ml bFGF (Life Technologies). We will refer to this media as MEF-CM. The day before

363 seeding onto micropatterns, the media was switched from mTeSR1 to MEF-CM. The next day, a

364 single cell suspension was prepared using accutase, and 5.5×10^4 cells in 2 ml of MEF-CM with

365 Rock-Inhibitor Y27672 (10 μM; StemCell Technologies) were seeded onto the micropatterned

366 coverslip. Custom-patterned glass coverslips (CYTOO) were placed in a 35 mm dish and coated

367 with 2 ml of 5 μg/ml Laminin-521 (LN521, Biolamina) in PBS (with calcium and magnesium)

368 for two hours at 37°C. After two hours, LN521 was washed out via serial dilutions by adding 6

369 ml PBS and removing 6 ml (6 dilutions). Then the remaining solution was removed entirely, and

370 cells were placed onto the coverslip and incubated at 37°C. After several hours, the media was

371 changed and the growth factors or small molecules added as indicated in the text.

372 *Reagents*. The following reagents were used to activate or inhibit signaling pathways: BMP4 (R

373 & D systems, dose as indicated in the text), Activin A (R & D systems, 10 ng/ml), Lefty (R & D

374 Systems, 500 ng/mL), SB431542 (Fisher Scientific, 10 μM), PD0325901 (ESI-BIO, 1 μM)

375 LDN-193189 (ESI-BIO, 200 nM), Y27672 (10μM, ESI-BIO) and IWP2 (EMD Millipore, 4 μM).

376 When increasing FGF levels, we used bFGF (Life Technologies, 100 ng/ml).

377 *Cell Lines*. All experiments in this work were performed with the hESC cell lines ESI017

378 (ESIBIO) or RUES2 (A gift of Ali Brivanlou, Rockefeller). GFP-SMAD4 cells were made from

379 the parental RUES2 line by using CRISPR/Cas9 genome engineering to fuse a cassette

380 containing a Puromycin resistance gene (PuroR), a t2a self-cleaving peptide, and GFP onto the

381 N-terminus of SMAD4 so that the locus produces both GFP-SMAD4 and PuroR. Subsequently,

382 cells were nucleofected with an ePiggyBac plasmid containing RFP-H2B driven by the CAG

383 promoter and also containing a Blasticidin (Bsd) resistance gene (ePB-B-CAG-RFP-H2B). Cells

384 were selected with 1 μg/ml Puromycin and 5 μg/ml Bsd. The Cdt1-RFP cell line was created by

385 nucleofecting ESI017 cells with an ePiggyBac construct encoding RFP-Cdt1 driven by the CAG

386 promoter and containing a Bsd resistence gene (ePB-B-CAG-RFP-Cdt1). Cells were selected

387 with 5 μg/ml Bsd. The CFP expressing cells were created by nucleofecting ESI017 cells with an

388 ePiggy construct encoding CFP-H2B driven by the CAG promoter and containing a Neomycin

389 resistance gene (ePB-N-CAG-CFP-hH2B). Cells were selected with 200 μg/ml G418.

390 *Immunostaining*. Coverslips were rinsed with PBS, fixed for 20 minutes using 4% PFA, rinsed

391 twice with PBS, and blocked for 30 minutes at room temperature. The blocking solution

392 contained 3% donkey serum and 0.1% Triton-X in 1X PBS. After blocking, the cells were

393   incubated with primary antibodies at 4°C overnight (see Table S1). The next day the cells were

394   washed three times with PBST (1X PBS with 0.1% Tween20) and incubated with secondary

395   antibodies (AlexaFluor488 cat#A21206, AlexaFluor555 cat#A31570, cat#A21432 and

396   AlexaFluor647 cat#A31571, dilution 1:500) and DAPI dye for 30 minutes at room temperature.

397   After secondary antibody treatment, samples were washed twice in PBST at room temperature.

398   Coverslips were then mounted in Fluoromount-G (Southern Biotech) and allowed to dry for

399   several hours.

400   *Imaging*. Entire fixed coverslips were imaged using tiled acquisition with a 20X, NA 0.75

401   objective on an Olympus IX83 inverted epifluorescence microscope. For live cell imaging

402   RUES2-GFP-SMAD4/RFP-H2B reporter cells were seeded on the micropattern as described

403   above and the patterned coverslip was then moved into a holder (CYTOO) to allow for imaging

404   through the coverslip without any intervening material. Images were acquired on an

405   Olympus/Andor spinning disk confocal microscope with either a 40X NA 1.25 silicon oil

406   objective or a 60X NA 1.35 oil objective. Approximately 4 z-planes were acquired at each

407   position every 12-17 minutes. For live cell imaging in standard culture conditions, reporter cells

408   were seeded onto ibidi slides as described above and imaged on an Olympus FV12 Laser

409   Scanning Confocal microscope with a 20X, NA 0.75 objective at time intervals of 20 minutes.

410   We typically acquired 2-4 hours of data before BMP4 stimulation and 20-24 hours for μColonies

411   and 40 hours for standard culture conditions afterwards.

412   *Image analysis*. Fixed cell experiments utilized large tiled images that were computationally

413   separated in smaller images of size 2048x2048. As the boundaries of these smaller images do not

414   align exactly with the individual images as originally acquired and stitched together by the

415   acquisition software, images presented may derive from 1-4 individual camera acquisitions.

416   Images of fixed cells acquired at 20X on the epifluorescence microscope were segmented using

417   custom software written in Matlab as described previously (Warmflash et al., 2012; Warmflash

418   et al., 2014) . Identified cells were grouped into μColonies based on the distance to their

419   neighbors. Cells within 80 microns were considered to be within a single μColony. We visually

420   inspected colony groupings for accuracy. Mean fluorescent intensities for each cell were

421   quantified and intensities for markers were normalized to the mean intensity of the DAPI stain in

422   each cell. All averages are taken over at least 100 cells. Images from live cell experiments were

423   first processed in ilastik (http://ilastik.org) to create nuclear and cellular masks. Custom

424   MATLAB software was used to postprocess these masks to separate touching cells and to

425   quantify both nuclear and cytoplasmic intensities.

426   Cell-cell communication model. In the conventional Ising Model, the Hamiltonian of the system

427   of atoms in magnetic field B can be written as a sum of energy due to interactions between the

428   neighboring spins and the energy due to magnetic field:

429

430
$$H = H_B + H_J = -B\sum_i^N s_i - \frac{J}{2}\sum_{i,j}^N s_i s_j \tag{1}$$

431

432   The probability P for the system to be in state σ is given by Boltzman distribution:

433

434
$$P(\sigma) = \frac{e^{-\beta H(\sigma)}}{Z} \tag{2}$$

435

436
$$Z = \sum_\sigma e^{-\beta H(\sigma)} \tag{3}$$

437

438   Where Z is the partition function of the system representing the sum of probabilities of all

439   possible states and β is the inverse temperature given by $1/k_B T$.

440   Note from the equations defining the model (1) − (3), that only products βB and βJ appear so that

441   we are free to choose units of energy such that β is equal to 1. We consider a system of size N

442   cells, where the external field B quantifies BMP4 concentration and the parameter J quantifies

443   the strength of the interactions between cells. Since the parameter J > 0, this interaction favors

444   configurations in which neighboring cells have the same identity. We make the simplifying

445   assumption that all cells in the μColony are neighbors which is justified by the small sizes of the

446   μColonies and the extensive cell rearrangements that occur during the observation period (see

447   Movie S1). If we take n cells to be in the CDX2+ state favored by the field B, then (N-n) cells

448   are in the SOX2+ state and the portion of the Hamiltonian due to external ligand is given by:

449

450
$$H_B = -(Bn - (N - n)B) = -(2n - N)B \tag{4}$$

451

452   The energy due to cell-cell interactions will be given by:

453

454 $$H_J = -J/2\{n(n-1)/2 + (N-n-1)(N-n)/2 - n(N-n)\} \tag{5}$$

455

456 where the first two terms in the sum represent the pairs of interacting cells, that are in the same

457 state (SOX2+ or CDX2+) and therefore contributing to H_J positively. The last term represents

458 the interactions between the SOX2+ and CDX2+ cells and therefore contributes negatively.

459 The total non-normalized probability for the μColony to have n cells in CDX2+ state and (N-n)

460 cells in SOX2+ state is then:

461

462 $$P(n,N) = C_n^N e^{B(2n-N)} e^{J/2((N-2n)^2-N)} \tag{6}$$

463

464 where C_n^N represents the number of combinations of n out of N ($C_n^N = N!/(n!\,(N-n)!)$).

465 The partition function Z is given by:

466

467 $$Z = \sum_{states} P(n,N) = \sum_{n=0}^{N} C_n^N e^{B(2n-N)} e^{J/2((N-2n)^2-N)} \tag{7}$$

468

469

470 These probabilities are then used to compute averages. For the results in Fig. 3, the average

471 fraction of cells in the CDX2+ state is:

472

473 $$f = \sum_{n=0}^{N} (n/N) \frac{P(n,N)}{Z} \tag{8}$$

474

475   To obtain the theoretical predictions to be compared to the experimental data, we repeat this

476   calculation for all values of N. We then minimized the sum of squares differences between the

477   model predictions and the data using a Monte-Carlo minimization algorithm coded in MATLAB.

478   We performed this fitting independently for each value of the BMP4 concentration, and also

479   performed a fit to all the data in which the value of J was fixed to be the same for all BMP4

480   concentrations, but the value of B at each concentration was considered a separate parameter (see

481   Figure S6E).

482

493   **Data Availability**

494   Custom-written Matlab codes for image segmentation and cell tracking of µColonies can be

495   found on GitHub in repository warmflasha/CellTracker and warmflasha/CellTracker60X.

496   **References**

497   **Arnold, S. J. and Robertson, E. J.** (2009). Making a commitment: cell lineage allocation and
498   axis patterning in the early mouse embryo. *Nat Rev Mol Cell Biol* **10**, 91–103.

499   **Berge, ten, D., Koole, W., Fuerer, C., Fish, M., Eroglu, E. and Nusse, R.** (2008). Wnt
500   signaling mediates self-organization and axis formation in embryoid bodies. *Cell Stem Cell*
501   **3**, 508–518.

502   **Bernardo, A. S., Faial, T., Gardner, L., Niakan, K. K., Ortmann, D., Senner, C. E., Callery,**
503   **E. M., Trotter, M. W., Hemberger, M., Smith, J. C., et al.** (2011). BRACHYURY and
504   CDX2 mediate BMP-induced differentiation of human and mouse pluripotent stem cells into

505   embryonic and extraembryonic lineages. *Cell Stem Cell* **9**, 144–155.

506   **Bier, E. and De Robertis, E. M.** (2015). EMBRYO DEVELOPMENT. BMP gradients: A
507   paradigm for morphogen-mediated developmental patterning. *Science* **348**, aaa5838–
508   aaa5838.

509   **Bolouri, H. and Davidson, E. H.** (2010). The gene regulatory network basis of the "community
510   effect," and analysis of a sea urchin embryo example. *Dev Biol* **340**, 170–178.

511   **Deglincerti, A., Etoc, F., Guerra, M. C., Martyn, I., Metzger, J., Ruzo, A., Simunovic, M.,**
512   **Yoney, A., Brivanlou, A. H., Siggia, E., et al.** (2016). Self-organization of human
513   embryonic stem cells on micropatterns. *Nat Protoc* **11**, 2223–2232.

514   **Dunn, N. R., Vincent, S. D., Oxburgh, L., Robertson, E. J. and Bikoff, E. K.** (2004).
515   Combinatorial activities of Smad2 and Smad3 regulate mesoderm formation and patterning
516   in the mouse embryo. *Development* **131**, 1717–1728.

517   **Etoc, F., Metzger, J., Ruzo, A., Kirst, C., Yoney, A., Ozair, M. Z., Brivanlou, A. H. and**
518   **Siggia, E. D.** (2016). A Balance between Secreted Inhibitors and Edge Sensing Controls
519   Gastruloid Self-Organization. *Dev Cell.* **39,** 302-315.

520   **Ferguson, E. L. and Anderson, K. V.** (1992). Decapentaplegic acts as a morphogen to organize
521   dorsal-ventral pattern in the Drosophila embryo. *Cell* **71**, 451–461.

522   **Gurdon, J. B.** (1988). A community effect in animal development. *Nature* **336**, 772–774.

523   **Horii, M., Li, Y., Wakeland, A. K., Pizzo, D. P., Nelson, K. K., Sabatini, K., Laurent, L. C.,**
524   **Liu, Y. and Parast, M. M.** (2016). Human pluripotent stem cells as a model of trophoblast
525   differentiation in both normal development and disease. *Proc Natl Acad Sci USA*
526   201604747.

527   **Karaulanov, E., Knöchel, W. and Niehrs, C.** (2004). Transcriptional regulation of BMP4
528   synexpression in transgenic Xenopus. *EMBO J* **23**, 844–856.

529   **Kurek, D., Neagu, A., Tastemel, M., Tüysüz, N., Lehmann, J., van de Werken, H. J. G.,**
530   **Philipsen, S., van der Linden, R., Maas, A., van IJcken, W. F. J., et al.** (2015).
531   Endogenous WNT Signals Mediate BMP-Induced and Spontaneous Differentiation of
532   Epiblast Stem Cells and Human Embryonic Stem Cells. *Stem Cell Reports* **4**, 114–128.

533   **Li, Y. and Parast, M. M.** (2014). BMP4 regulation of human trophoblast development. *Int. J.*
534   *Dev. Biol.* **58**, 239–246.

535   **Li, Y., Moretto-Zita, M., Soncin, F., Wakeland, A., Wolfe, L., Leon-Garcia, S., Pandian, R.,**
536   **Pizzo, D., Cui, L., Nazor, K., et al.** (2013). BMP4-directed trophoblast differentiation of
537   human embryonic stem cells is mediated through a ΔNp63+ cytotrophoblast stem cell state.
538   *Development* **140**, 3965–3976.

539   **Muñoz-Descalzo, S., Rué, P., Garcia-Ojalvo, J. and Martinez Arias, A.** (2012). Correlations

540   between the levels of Oct4 and Nanog as a signature for naïve pluripotency in mouse
541   embryonic stem cells. *Stem Cells* **30**, 2683–2691.

542   **Peerani, R., Rao, B. M., Bauwens, C., Yin, T., Wood, G. A., Nagy, A., Kumacheva, E. and**
543   **Zandstra, P. W.** (2007). Niche-mediated control of human embryonic stem cell self-renewal
544   and differentiation. *EMBO J* **26**, 4744–4755.

545   **Robertson, E. J.** (2014). Dose-dependent Nodal/Smad signals pattern the early mouse embryo.
546   *Semin Cell Dev Biol* **32**, 73–79.

547   **Saka, Y., Lhoussaine, C., Kuttler, C., Ullner, E. and Thiel, M.** (2011). Theoretical basis of the
548   community effect in development. *BMC Syst Biol* **5**, 54.

549   **Sakaue-Sawano, A., Kurokawa, H., Morimura, T., Hanyu, A., Hama, H., Osawa, H.,**
550   **Kashiwagi, S., Fukami, K., Miyata, T., Miyoshi, H., et al.** (2008). Visualizing
551   spatiotemporal dynamics of multicellular cell-cycle progression. *Cell* **132**, 487–498.

552   **Schmierer, B. and Hill, C. S.** (2005). Kinetic analysis of Smad nucleocytoplasmic shuttling
553   reveals a mechanism for transforming growth factor beta-dependent nuclear accumulation of
554   Smads. *Mol Cell Biol* **25**, 9845–9858.

555   **Schuler-Metz, A., Knöchel, S., Kaufmann, E. and Knöchel, W.** (2000). The homeodomain
556   transcription factor Xvent-2 mediates autocatalytic regulation of BMP-4 expression in
557   Xenopus embryos. *J Biol Chem* **275**, 34365–34374.

558   **Sorre, B., Warmflash, A., Brivanlou, A. H. and Siggia, E. D.** (2014). Encoding of temporal
559   signals by the TGF-β pathway and implications for embryonic patterning. *Dev Cell* **30**, 334–
560   342.

561   **Tang, C., Ardehali, R., Rinkevich, Y., Seita, J., Lee, A. S., Mosley, A. R., Drukker, M.,**
562   **Weissman, I. L. and Soen, Y.** (2012). isolation of primitive endoderm, mesoderm, vascular
563   endothelial and trophoblast progenitors from human pluripotent stem cells. *Nat Biotechnol*
564   **30**, 531–542.

565   **Tucker, J. A., Mintzer, K. A. and Mullins, M. C.** (2008). The BMP signaling gradient patterns
566   dorsoventral tissues in a temporally progressive manner along the anteroposterior axis. *Dev*
567   *Cell* **14**, 108–119.

568   **van den Brink, S. C., Baillie-Johnson, P., Balayo, T., Hadjantonakis, A.-K., Nowotschin, S.,**
569   **Turner, D. A. and Martinez Arias, A.** (2014). Symmetry breaking, germ layer
570   specification and axial organisation in aggregates of mouse embryonic stem cells.
571   *Development* **141**, 4231–4242.

572   **Warmflash, A., Sorre, B., Etoc, F., Siggia, E. D. and Brivanlou, A. H.** (2014). A method to
573   recapitulate early embryonic spatial patterning in human embryonic stem cells. *Nat Meth* **11**,
574   847–854.

575   **Warmflash, A., Zhang, Q., Sorre, B., Vonica, A., Siggia, E. D. and Brivanlou, A. H.** (2012).

576 Dynamics of TGF-β signaling reveal adaptive and pulsatile behaviors reflected in the nuclear
577 localization of transcription factor Smad4. *Proc Natl Acad Sci USA* **109**, E1947–56.

578 **Wilson, P. A., Lagna, G., Suzuki, A. and Hemmati-Brivanlou, A.** (1997). Concentration-
579 dependent patterning of the Xenopus ectoderm by BMP4 and its signal transducer Smad1.
580 *Development* **124**, 3177–3184.

581 **Winnier, G., Blessing, M., Labosky, P. A. and Hogan, B. L.** (1995). Bone morphogenetic
582 protein-4 is required for mesoderm formation and patterning in the mouse. *Genes Dev* **9**,
583 2105–2116.

584 **Xu, R.-H., Chen, X., Li, D. S., Li, R., Addicks, G. C., Glennon, C., Zwaka, T. P. and
585 Thomson, J. A.** (2002). BMP4 initiates human embryonic stem cell differentiation to
586 trophoblast. *Nat Biotechnol* **20**, 1261–1264.

587 **Yu, P., Pan, G., Yu, J. and Thomson, J. A.** (2011). FGF2 sustains NANOG and switches the
588 outcome of BMP4-induced human embryonic stem cell differentiation. *Cell Stem Cell* **8**,
589 326–334.

590

591 **Figure legends**

592 **Figure 1. BMP causes differentiation of µColonies to a single fate with a sharp threshold**.

593 (A) Representative image of stem cells in µColonies. (B) Representative distribution of colony

594 sizes. (C) Fractions of SOX2, CDX2 or BRA positive cells upon differentiation with BMP4 for

595 42 hours. (D) Example images of immunofluorescence for CDX2 and SOX2 at the indicated

596 BMP4 doses. (E) Scatter plots of SOX2 versus CDX2 markers for indicated BMP4

597 concentrations. Each dot corresponds to a single cell while the color code indicates the size of

598 the colony containing that cell. Scale bars 50 µm. See also Fig. S1 and S2.

599 **Figure 2. In standard culture, treatment with BMP4 reveals a morphogen effect that**

600 **depends on Nodal signaling and cell density.** (A) Representative images showing SOX2,

601 CDX2 and BRA differentiation in response to two doses of BMP4. Scale bar 50 µm. (B-C) Mean

602 expression of SOX2, BRA and CDX2 markers as a function of BMP4 concentrations with (C)

603 and without (B) 10µm SB431542. The values in (B) and (C) are normalized to the maximum

604 over both sets which were performed in the same experiment. (D-E) Mean expression of SOX2,

605 BRA and CDX2 markers after differentiation with 2 (D) or 10 (E) ng/ml BMP4 with varied

606 initial seeding density. The values in (D) and (E) are normalized to the maximum over the two

607 sets which were performed in the same experiment. Dotted lines represent the levels of

608   expression of the indicated marker under pluripotency conditions. All differentiation

609   experiments were conducted for 42 hours. See also Fig. S3.

610   **Figure 3. A community effect enforces a common fate in μColonies.** (A) Representative

611   image demonstrating the community effect in differentiated conditions (1 ng/ml BMP4). Scale

612   bar 50 μm. (B) Distributions of SOX2 and CDX2 expression in cells of one- and seven-cell

613   colonies in undifferentiated conditions. (C) The fraction of cells expressing a given gene is

614   shown with fits to the Ising-like model. Error bars represent the standard deviation over at least

615   three biological replicates. See also Fig. S5.

616   **Figure 4. Clonal expansion or cell cycle effects cannot explain the community effect.** Mean

617   total DNA content (A) and fraction of cells in the G1 phase of the cell cycle (B) as a function of

618   colony size. In (A) the error bars represent the standard error of the mean calculated separately

619   for each colony size. For (B) the error bars were calculated using bootstrapping method. (C)

620   Representative images of μColonies containing both CFP-positive and CFP-negative cells in

621   pluripotent or BMP4-treated conditions. Scale bar 50 μm. (D) Analysis of mean SOX2 or CDX2

622   levels in the mixed colonies in pluripotent (blue stars) or BMP-treated conditions (red stars).

623   (Top row) 4-8 cell colonies containing both CFP-positive and CFP-negative cells were identified

624   and the mean SOX2 or CDX2 levels was computed separately for the CFP-positive and the CFP-

625   negative cells. (Bottom row) In the same mixed colonies, the cells were randomly divided into

626   two groups and the mean levels of SOX2 or CDX2 were computed for each group of cells.

627   **Figure 5. Reinforcement of the BMP signal underlies the community effect in differentiated**

628   **cells.** (A) Representative images of reporter cells. Scale bar 10 μm (see Movie S1). (B)

629   Representative trajectories for the one- and two-cell colonies treated with 10 ng/ml BMP4. (C)

630   Mean signaling trajectories for one and two cell colonies. (D) –(F) Histograms of mean signaling

631   intensity in individual cells over the indicated time intervals. (G) Cells were classified as high or

632   low expressing for CDX2. The mean signaling is shown in each case. (H) Signaling trajectories

633   were similarly binarized as high or low signaling and the fraction of cells with high or low

634   CDX2 examined as function of the signaling level. Due to difficulty tracking individual cells for

635   42 hours, cells were fixed and analyzed for CDX2 after 24 hours in BMP4. In panels (C) and (H)

636   error bars represent standard error of the mean over trajectories. (I)The same colonies from panel

637   (H) that contained one cell at the time of BMP4 stimulation were grouped depending on whether

638   that cell later divided and then evaluated for CDX2 expression.

639   **Figure 6. Cells fates correlate with the duration of signaling rather than initial response to**

640   **BMP4.** (A) Representative images of reporter cells in standard culture conditions at the indicated

641   time points following BMP4 treatment. Scale bar 20 μm. Images were acquired every 20

642   minutes. (B-D) (Top row) The BMP pathway was stimulated with BMP4 or inhibited with

643   Noggin as indicated in the legends. The GFP-SMAD4 reporter line was used to determine the

644   signaling activity as a function of time. (Bottom row) The same cells were then fixed and

645   analyzed for CDX2 expression. In (C), the 1→10 and 10→1 conditions, indicate wells that were

646   treated with 1 ng/ml or 10 ng/ml BMP4 and then the media was swapped between those two

647   wells at 3 hours. In (D), the 10→250 noggin, indicates wells in which the media containing

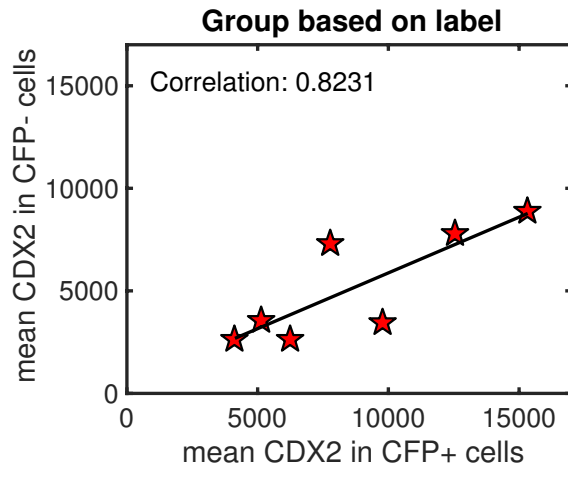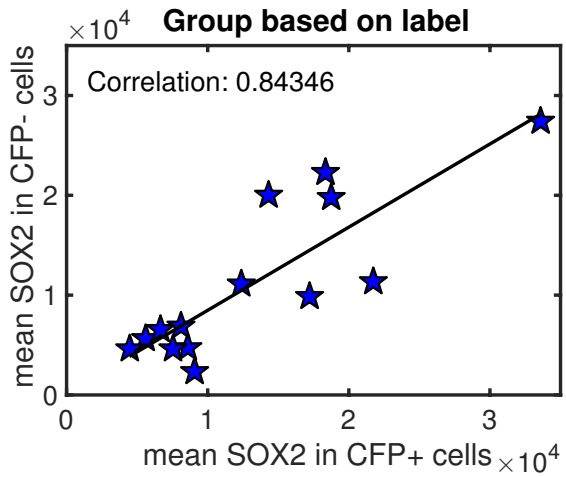648   10ng/ml BMP4 was replaced with media containing 250 ng/ml Noggin at the listed times.

649
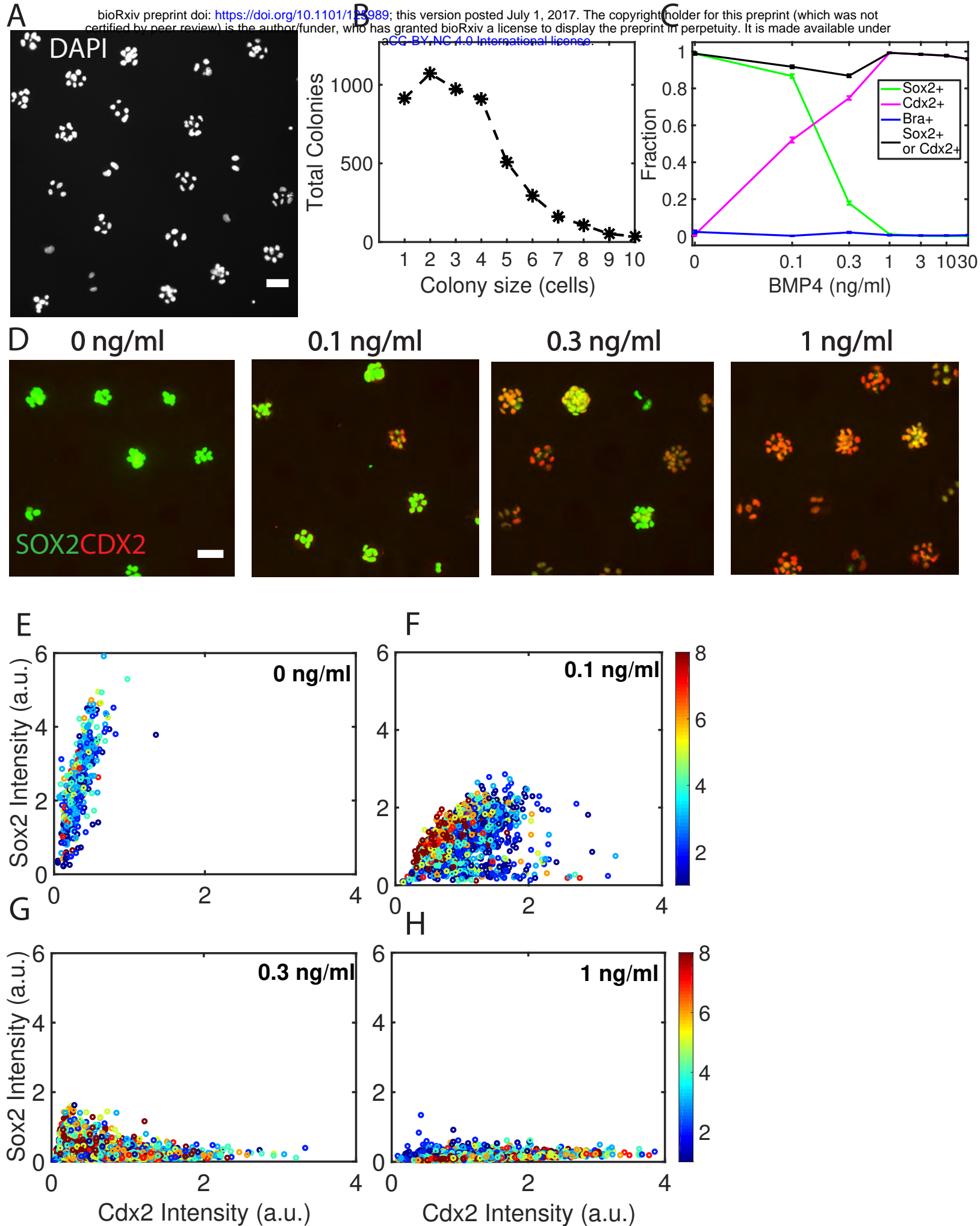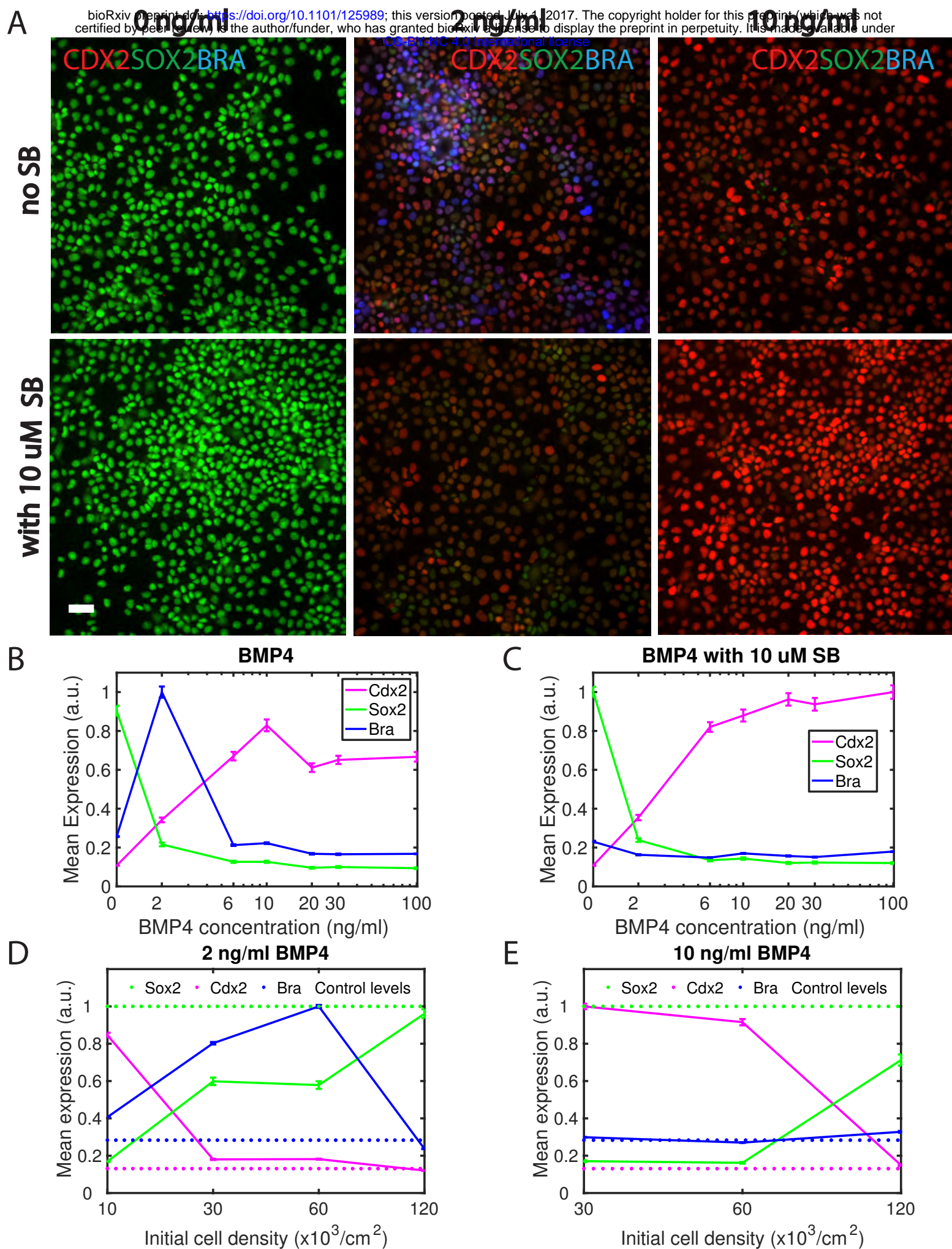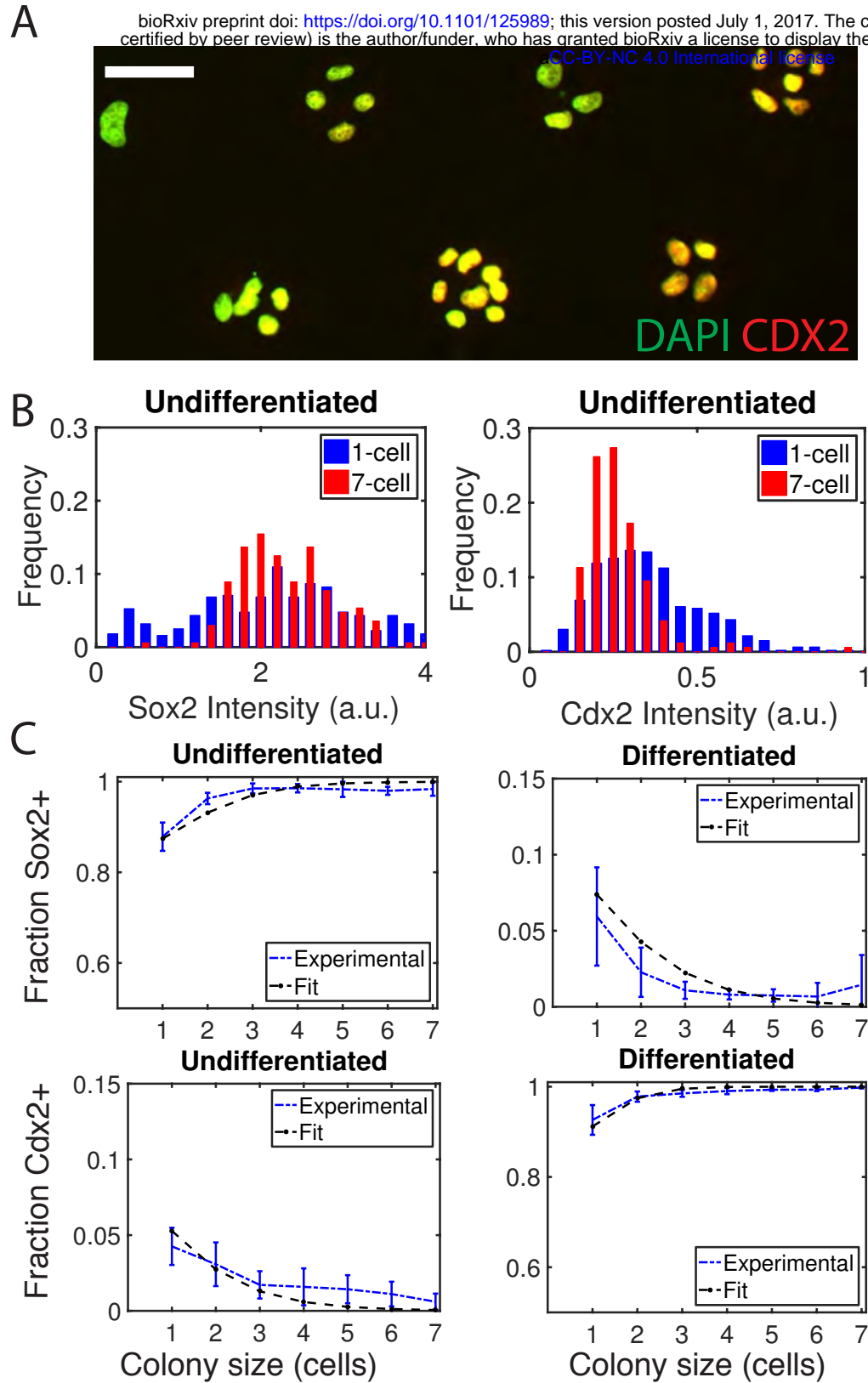
FIGURE 1

FIGURE 2

FIGURE 3
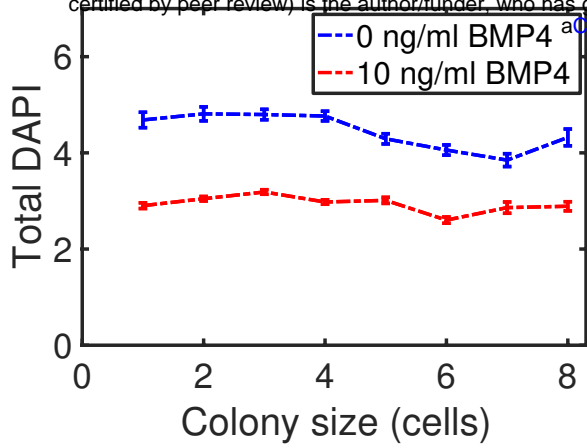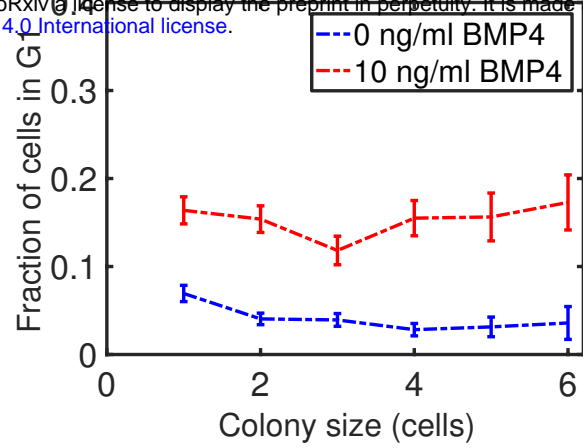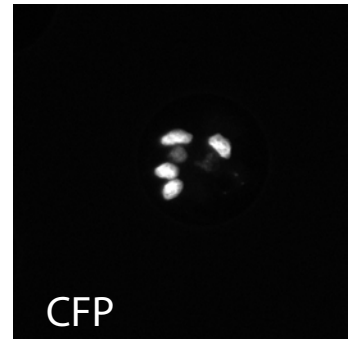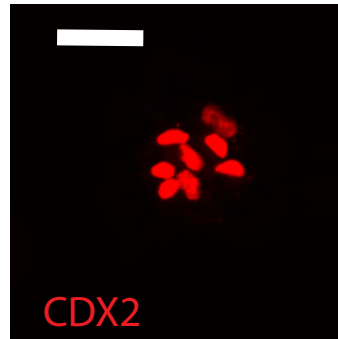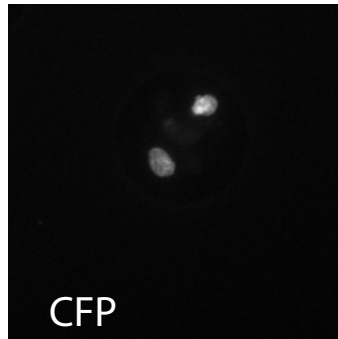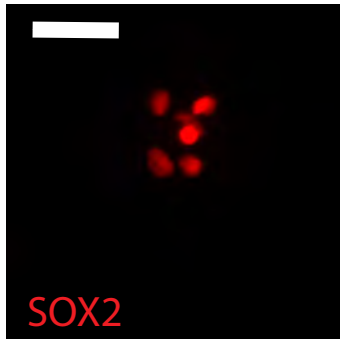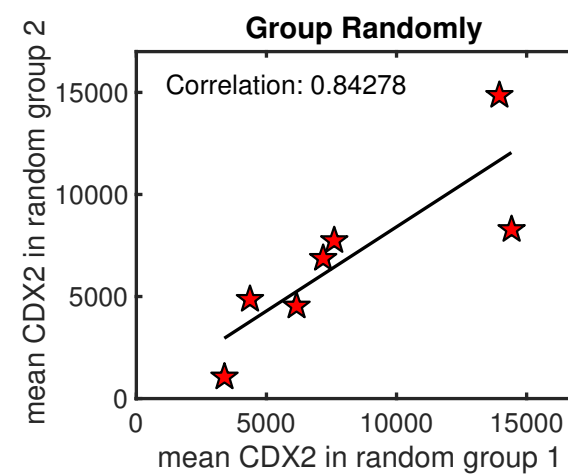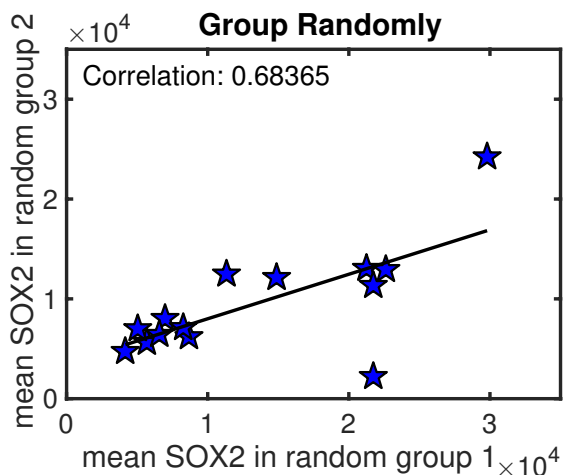
FIGURE 4

FIGURE 5

FIGURE 6